JOURNAL OF MOLECULAR SPECTROSCOPY 167, 191–204 (1994)

The Microwave Spectrum and Structure of the CH_3OH–CO Dimer[1]

F. J. LOVAS, S. P. BELOV,[2] M. YU. TRETYAKOV,[2]
J. ORTIGOSO, AND R. D. SUENRAM

Molecular Physics Division, National Institute of Standards and Technology, Gaithersburg, Maryland 20899

The rotational spectrum of CH_3OH–CO has been observed in the region 7–18 GHz with a pulsed-beam Fabry–Perot cavity Fourier-transform microwave spectrometer. In order to obtain detailed structural information the spectra of CH_3OH, CH_3OD, CD_3OH, and CD_3OD combined with CO and ^{13}CO were examined. Each of the isotopic species studied exhibits two states, which are interpreted as *A* and *E* symmetry states arising from internal rotation of the methyl group. The *E*-state assignments were verified by observing their first-order Stark effect. The structure of the complex is a bent hydrogen bond of the carbon atom of CO at a distance of 2.41 Å from the hydroxyl hydrogen of methanol and planar heavy atoms. The effective barrier to internal rotation for CH_3OH–CO, V_3 = 183.0 cm^{-1}, is one-half of the value for the methanol monomer.

I. INTRODUCTION

The reaction mechanism involved in the conversion of *m*ethanol *t*o *g*asoline (MTG) over a zeolite catalyst (MTG process) (*1*) has generated considerable interest, although much controversy still remains over the particular steps which lead to the formation of the first C–C bond. The preferred process for the conversion of methanol to gasoline uses a zeolite catalyst (SiO_2/Al_2O_3) (*2, 3*), although methanol has also been shown to be efficiently converted to hydrocarbons over a number of other catalysts, such as acidic materials like a mixture of polyphosphoric acid and trimethyl phosphate (*4*).

It is generally accepted that the initial step in the MTG process starts with methanol being absorbed onto a Brönsted-acid site, HOZ, of the catalyst as a methyloxonium ion, $CH_3OH_2^+$ ^-OZ, where OZ stands for the zeolite structure. Elimination of water yields a surface methoxy group (CH_3OZ) (*5, 6*), or reaction with another methanol molecule (from the gas phase or perhaps absorbed on a neighboring site) yields dimethyl ether and water, as shown in Fig. 1. Dimethyl ether, in turn, can be absorbed onto an acid site giving a dimethyl oxonium ion, which can further react with methanol to yield a trimethyloxonium ion, $(CH_3)_3O^+$.

The mechanism for obtaining C–C bonds from the surface oxonium ions and methoxy groups has generated considerable study and debate (*3*). Olah (*7*) has suggested an oxonium ylide mechanism whereby one of the methyl groups of the oxonium ion becomes deprotonated and then undergoes rearrangement to yield a carbon–carbon bond (*7, 8*). Strong support for this mechanism has come from studies by Olah and co-workers (*9, 10*) and Rimmelin and co-workers (*11*) on model oxonium salts.

[1] Contribution of the National Institute of Standards and Technology (formerly National Bureau of Standards). Not subject to copyright.

[2] Guest workers, 1992–1993. Permanent address: Institute of Applied Physics, Nizhni Novgorod, Russia.

0022-2852/94 $6.00

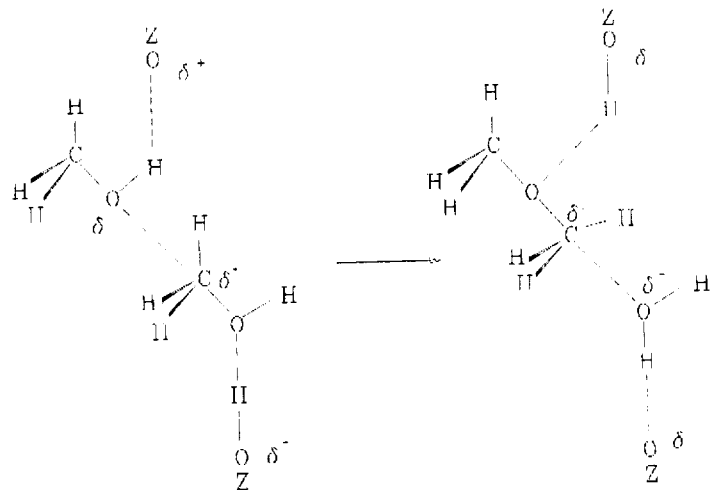

FIG. 1. Mechanism for the first step in the MTG process, which shows the addition of a second molecule to a surface-adsorbed methanol and yielding dimethyl ether plus water.

Following Pearson's initial suggestion (*4*), Kagi (*12*), Ono and Mori (*6*), and Baba *et al.* (*13*) have favored a C–C bond forming mechanism which invokes the pentacoordinate carbon species of Olah *et al.* (*9, 10*). In this picture, the presence of surface oxonium ions furnishes a source of "mobile" methyl cations, CH_3^+, which attack the carbon site of a nearby absorbed dimethyl ether. Proton elimination results in the formation of methylethyl ether, which can then undergo further reactions with other carbocations. Chang and co-workers (*14, 15*) and others (*16, 17*) have stressed the importance of carbenes in the MTG and related processes. Chang and Silvestri (*14*) invoke a concerted mechanism of methylene insertion into a C–H bond of methanol or dimethyl ether. Here, the methylene is formed by α elimination from methanol.

A recent alternative mechanism has been proposed by Jackson and Bertsch (*18*). In their picture, carbon monoxide formed by dehydrogenation of methanol produces an S_N2 displacement of water from a surface oxonium ion ($CO + CH_3OH_2^+ \rightarrow CH_3CO^+$) to form an acylium ion. This acylium ion eliminates a hydrogen ion to form ketene, which undergoes further reaction with oxonium ions until CO is eliminated and propene is formed. Munson *et al.* (*19*) have questioned this mechanism after finding no evidence that added CO (from formic acid decomposition) accelerates the MTG reaction rate. In fact, their isotopic labeling experiments show no incorporation of ^{13}C from ^{13}C-labeled formic acid into the hydrocarbon products.

One problem in studying the MTG mechanism experimentally is the difficulty of obtaining reliable information on processes within the zeolite matrix. Such difficulties might be avoided by constructing model gas-phase systems which closely mimic the solid-phase MTG reaction environment. In the idealized experiments surface-bound methanol would be simulated by binding various protonic acids, such as HF, HCl, or H_2O, to the O atom of methanol and the high sensitivity and species selectivity of pulsed-supersonic-nozzle Fourier-transform microwave techniques can then be used to obtain rapid and reliable information on the structures and large-amplitude motions of these gas-phase "reaction" complexes. Further interactions of these dimeric species

mimicking "surface-bound" methanol would be studied with the addition of CH_3OH or CO, each of which is a known or postulated intermediate in the MTG process. Such studies could give a detailed picture of the orientation of various reactant species along the entrance channel to reaction and, in favorable cases, give information about the transition state for reaction. This approach has been used previously to investigate the reactions of ozone with ethylene and acetylene (*20–22*), ketene with acetylene (*23*), and proton-transfer reactions in ammonium halides (*24*) and cyanides (*25, 26*). The present study of CH_3OH–CO was undertaken as a preliminary step in examining where CO would bond to methanol, and subsequently to examine the CO–CH_3OH–HF species. A parallel study of methanol–water and the methanol dimer is in progress.

II. EXPERIMENTAL DETAILS

Spectral measurements were carried out with a pulsed-beam Fabry–Perot cavity, Fourier-transform microwave spectrometer (*27, 28*) of the Balle–Flygare type (*29*) in the frequency region 8–24 GHz. A dual-inlet pulsed solenoid valve was used to deliver a supersonic molecular beam from a mixture of about 1 volume% CO and CH_3OH, entrained in separate samples with Ar carrier gas, at a total pressure of 100 kPa (1 atm) to the center of a Fabry–Perot cavity. Molecular-beam pulses from a 0.5-mm orifice of 200- to 400-μs duration were employed with repetition rates up to 35 Hz. The molecular complex was polarized by a short microwave pulse when the microwave frequency was near resonant ($\Delta\nu < 400$ kHz) with a rotational transition of the complex. The free-induction decay signal from the cavity was then digitized in 0.5-μs increments for 512 channels. Typically, 200–2000 pulses were signal averaged, after subtracting a background microwave pulse from each signal pulse, in order to yield reasonable signal-to-noise ratios. The averaged data were then Fourier transformed to obtain the power spectrum with a resolution element of 3.9063 kHz/point and linewidth of 10–15 kHz. The measurement precision and accuracy is estimated to be 4 kHz, which is the resolution element. In order to confirm the assignment for the K_a rotational quantum number, Stark fields were applied to the molecular beam by two parallel plates (26 × 26 cm) with a separation of about 26 cm by using voltages up to +5 and −5 kV on each plate.

To produce the various isotopically substituted CH_3OH–CO dimers, we used commercially available samples of normal CH_3OH and CO, CH_3OD, CD_3OD, and ^{13}CO. The dimers containing CD_3OH were observed through H/D atom exchange of CD_3OD in the nozzle inlet system. The dual inlet served to introduce the CO/Ar and CH_3OH/Ar samples to the nozzle in a continuous flow manner, independently. This allowed chemical characterization of spectral transitions detected. In addition to the CH_3OH–CO species, other known dimeric species observed were CO–H_2O (*30*) and Ar–CH_3OH (*28*), and subsequently methanol dimer (*31*). It was relatively easy to distinguish between each of these by alternately cutting off the flow of each of the inlets or by using Ne as carrier gas.

III. OBSERVED SPECTRUM AND ASSIGNMENT

The initial searches provided several groups of *a*-type *R*-branch transitions which exhibited the second-order Stark effect characteristic of $K_{-1} = 0$ and 1 transitions. Each of these transitions was accompanied by an equally intense transition which showed a first-order Stark effect. The latter transitions were assigned to the *E* state

arising from methyl internal rotation, and the former are assigned to the *A* state. Three groups of *R*-branch transitions were measured for each isotopic species, and eventually several *b*-type transitions for both *A* and *E* states. Table I lists the measurements for CH_3OH–CO and CH_3OD–CO, Table II gives the CH_3OH–^{13}CO and CH_3OD–^{13}CO species, and Table III provides the assignments for the CD_3OH–CO and CD_3OD–CO species.

While the assignment of the spectrum was rather straightforward, the spectral analysis proved to be more difficult. The initial analysis employed the usual Watson Hamiltonian (*32*). With this formulation, only the *A*-state transitions could be fit close to the experimentally measured uncertainty when the standard Watson asymmetric-top Hamiltonian was used. It resulted in the molecular constants shown in Table IV. A combined fit of the *A*- and *E*-state lines with a simple IAM (internal axis method) treatment of the internal rotation splittings was much poorer, with deviations between observed and calculated transitions of up to 5 MHz for CH_3OH–CO and CH_3OD–CO, and about 0.5 MHz for CD_3OH–CO and CD_3OD–CO. Since this simple model did not allow for higher order terms, e.g., centrifugal distortion of the internal rotor terms, we turned to the model developed by Godefroid and Kleiner (*33–35*) which is discussed in Section IV.

TABLE I

Transition Frequencies of CH_3OH–CO and CH_3OD–CO[a]

J'	K_a'	K_c'	J	K_a	K_c	Sym	CH_3OH–CO ν(MHz)	O–C[b] A+E	O–C[b] A	CH_3OD–CO ν(MHz)	O–C[b] A+E	O–C[b] A
2	1	2	1	1	1	A	7168.910	-13	-3	-		
2	0	2	1	0	1	A	7277.023	22	5	-		
2	1	1	1	1	0	A	7390.173	-34	-4	-		
4	1	4	5	0	5	A	8109.992	1	4	7585.564	-2	0
3	1	3	2	1	2	A	10752.041	-14	-1	10730.798	-12	-6
3	0	3	2	0	2	A	10913.412	12	1	10892.995	4	4
3	1	2	2	1	1	A	11083.635	-26	-4	11064.465	-23	-10
3	1	3	4	0	4	A	11954.168	-7	-1	11424.191	-2	-2
4	1	4	3	1	3	A	14333.581	-7	0	14305.422	2	5
4	0	4	3	0	3	A	14547.272	0	3	14520.160	3	5
4	1	3	3	1	2	A	14775.155	35	5	14749.756	16	7
2	1	2	3	0	3	A	15749.398	6	1	15213.545	4	2
5	1	5	4	1	4	A	17913.006	21	2	17878.045	9	1
5	0	5	4	0	4	A	18177.754	-18	-5	18144.037	-9	-8
2	1	2	1	1	1	E	7263.555	20*		-		
2	0	2	1	0	1	E	7270.018	7		-		
2	0	2	1	0	1	E	7286.490	51*		-		
4	1	4	5	0	5	E	7348.525	2		-		
4	1	3	5	0	5	E	9689.441	-9		-		
3	1	3	2	1	2	E	10873.656	8		10835.737	7	
3	0	3	2	0	2	E	10903.002	2		10886.779	0	
3	1	2	2	1	1	E	10948.429	30		10950.033	1	
3	1	3	4	0	4	E	11047.522	7		-		
3	1	2	4	0	4	E	13221.659	21		12399.829	7	
4	1	4	3	1	3	E	14461.900	3		14401.191	8	
4	0	4	3	0	3	E	14533.560	-4		14511.972	4	
4	1	3	3	1	2	E	14628.680	-20		14641.318	-5	
2	1	2	3	0	3	E	14707.422	-9		14595.437	-8	
2	1	1	3	0	3	E	16806.791	-12		15961.751	-7	
5	1	5	4	1	4	E	18030.052	-14		17952.118	-8	
5	0	5	4	0	4	E	18160.895	7		18133.952	-4	
1	1	1	2	0	2	E	-			18237.357	8	

[a]Estimated measurement uncertainty, one std. deviation, is 4 kHz.

[b]Observed minus calculated frequency given in kHz. The first column shows values for the combined A and E state fit and the second shows values for the A state. The * indicates transitions not included in the fit.

TABLE II

Transition Frequencies of CH_3OH–^{13}CO and CH_3OD–^{13}CO[a]

J′	K_a′	K_c′	J	K_a	K_c	Sym	CH_3OH–^{13}CO ν(MHz)	O–C[b] A+E	O–C[b] A	CH_3OD–^{13}CO ν(MHz)	O–C[b] A+E	O–C[b] A
4	1	4	5	0	5	A	8300.199	1	0	-		
3	1	3	2	1	2	A	10655.198	-10	-1	10633.409	-12	-9
3	0	3	2	0	2	A	10813.395	20	3	10792.398	3	5
3	1	2	2	1	1	A	10980.572	-37	-5	10960.757	-16	-6
3	1	3	4	0	4	A	12107.028	-7	-2	11652.869	2	2
4	1	4	3	1	3	A	14204.500	-7	-1	14175.611	8	2
4	0	4	3	0	3	A	14414.006	1	0	14386.137	8	11
4	1	3	3	1	2	A	14637.795	27	4	14611.530	11	0
2	1	2	3	0	3	A	15865.838	6	1	15405.574	-2	-2
5	1	5	4	1	4	A	17751.726	14	2	17715.854	33*	3
5	0	5	4	0	4	A	18011.329	-16	-3	17976.664	-6	-10
5	1	4	4	1	3	A	-			18259.884	72*	3
3	1	3	2	1	2	E	10774.833	7		10736.894	0	
3	0	3	2	0	2	E	10803.375	-5		10786.395	5	
3	1	2	2	1	1	E	10847.783	15		10848.056	-5	
3	1	3	4	0	4	E	11208.952	4		11143.580	0	
3	1	2	4	0	4	E	13355.833	11		-		
4	1	4	3	1	3	E	14330.968	6		14270.453	-1	
4	0	4	3	0	3	E	14400.814	-3		14378.207	-1	
4	1	3	3	1	2	E	14493.756	-15		14504.410	8	
2	1	2	3	0	3	E	14834.935	-4		-		
2	1	1	3	0	3	E	16908.860	-11		-		
5	1	5	4	1	4	E	17867.366	-12		17789.538	1	
5	0	5	4	0	4	E	17995.098	17		17966.903	-2	
5	1	4	4	1	3	E	18154.818	-3		18170.843	-3	

[a]Estimated measurement uncertainty, one std. deviation, is 4 kHz.

[b]Observed minus calculated frequency given in kHz. The first column shows values for the combined A and E state fit and the second shows values for the A state.

TABLE III

Transition Frequencies of CD_3OH–CO and CD_3OD–CO[a]

J′	K_a′	K_c′	J	K_a	K_c	Sym	CD_3OH–CO ν(MHz)	O–C[b] A+E	O–C[b] A	CD_3OD–CO ν(MHz)	O–C[b] A+E	O–C[b] A
3	1	3	2	1	2	A	10055.872	-6	-5	10032.645	-19	-1
3	0	3	2	0	2	A	10207.460	7	4	10185.788	0	-6
3	1	2	2	1	1	A	10366.798	3	-2	10347.214	6	3
2	1	2	3	0	3	A	10605.422	3	5	10237.410	11	6
4	1	4	3	1	3	A	13405.075	-2	-1	13374.298	-3	7
4	0	4	3	0	3	A	13605.541	7	7	13576.775	-8	-10
4	1	3	3	1	2	A	13819.022	1	0	13793.102	7	8
1	1	1	2	0	2	A	14107.963	-3	-5	13733.810	-11	-4
5	1	5	4	1	4	A	16751.918	4	2	16713.733	8	-8
5	0	5	4	0	4	A	16999.848	-8	-5	16964.145	14	15
5	1	4	4	1	3	A	17268.353	-3	1	17236.238	-9	-9
3	1	3	2	1	2	E	10083.410	1		10042.556	-6	
3	0	3	2	0	2	E	10204.815	48*		10184.346	5	
3	1	2	2	1	1	E	10334.195	-8		10334.540	-17	
2	1	2	3	0	3	E	10500.748	-14		10194.830	-10	
4	1	4	3	1	3	E	13418.160	5		13378.153	30	
4	0	4	3	0	3	E	13601.987	-3		13574.883	10	
4	1	3	3	1	2	E	13799.206	-6		13785.614	6	
1	1	1	2	0	2	E	13952.980	14		13663.876	10	
5	1	5	4	1	4	E	16757.984	0		16715.137	-15	
5	0	5	4	0	4	E	16995.480	-7		16961.756	-19	
5	1	4	4	1	3	E	17253.914	10		17230.256	7	

[a]Estimated measurement uncertainty, one std. deviation, is 4 kHz.

[b]Observed minus calculated frequency given in kHz. The first column shows values for the combined A and E state fit and the second shows values for the A state. The * indicates transitions not included in the fit.

TABLE IV

Rotational Constants for the A State of CH_3OH–CO, CH_3OH–^{13}CO, CH_3OD–CO, and CH_3OD–^{13}CO (in MHz)

Parameter	CH_3OH–CO	CH_3OH–^{13}CO	CH_3OD–CO	CH_3OD–^{13}CO	CD_3OH–CO	CD_3OD–CO
A	28644.468(7)[a]	28641.202(8)[a]	28085.827(2)[a]	28157.226(15)[a]	22667.482(7)[a]	22275.78(2)[a]
B	1874.865(2)	1857.142(2)	1871.788(4)	1853.949(3)	1753.839(2)	1750.813(5)
C	1764.153(1)	1748.507(1)	1760.385(3)	1744.661(3)	1650.001(2)	1645.761(5)
Δ_J	0.021051(14)	0.020732(17)	0.01957(4)	0.01925(3)	0.02341(2)	0.02154(4)
Δ_{JK}	-0.5450(3)	-0.5644(3)	-0.5759(7)	-0.5922(3)	-0.4308(5)	-0.4635(11)
δ_J	0.002498(19)	0.002432(22)	0.002495(49)	0.002395(33)	0.002735(22)	0.002735(5)

[a] Uncertainties shown in parentheses refers to the last digits and are one standard deviation.

IV. INTERNAL ROTATION ANALYSIS

The difficulty in fitting the microwave spectrum of methanol–CO might arise from several large-amplitude motions, e.g., torsional motion of the CH_3 groups, or overall rotation of the CO subunit. One expects that the CH_3 groups would provide internal rotation splittings even in the ground state since it is relatively unhindered. Thus, if other motions are present in this dimer, it is not obvious how to treat it from an *a priori* viewpoint. The obvious first-order treatment is to deal with CH_3 internal rotation at the highest level of theory available. If this is not successful then further motions must be examined.

For the internal rotation problem, we used programs developed by Kleiner *et al.* (*33–35*), which are based on the IAM method described by Liang *et al.* (*36*). The method operates by first diagonalizing the pure torsional part of the Hamiltonian operator, and then, using these eigenvectors multiplied by rotational basis functions, the rotation–torsion matrix is constructed and diagonalized.

After several attempts at fitting the observed transitions by using different sets of molecular constants, we were able to fit the spectra with a root-mean-square deviation between 5 and 15 kHz, depending on the isotopic species. The Hamiltonian employed was

$$H = AP_a^2 + BP_b^2 + CP_c^2 + D_{ab}[P_aP_b + P_bP_a] - \Delta_J\mathbf{P}^4 - \Delta_{JK}\mathbf{P}^2P_a^2 - \delta_J[2\mathbf{P}^2(P_b^2 - P_c^2)] + (1 - \cos 3\gamma)[(1/2)V_3 + F_v\mathbf{P}^2 + k_5\mathbf{P}_a^2 + c_2(P_b^2 - P_c^2)] + P_\gamma\{FP_\gamma + \rho P_a + L_vP_a\mathbf{P}^2 + c_4[(P_b^2 - P_c^2)P_a + P_a(P_b^2 - P_c^2)]\}. \quad (1)$$

See Ref. (*35*) for a definition of the above parameters. These molecular constants should be considered "effective" and they include the dependence of both the barrier, V_3, and the dimensionless parameter, ρ, on the rotational quantum numbers J and K. Table V summarizes the number of transitions fitted, the number of parameters employed, and the rms deviation for each of the isotopic species of methanol–carbon monoxide. The values for the barrier, V_3, are also shown. The invariance of the effective barrier upon isotopic substitution is evident and provides confidence in the model employed. However, there is a relationship that the molecular constants should fulfill. This constraint can be written as a relation between the rotational constants and the internal rotation parameters F and ρ,

$$AB - D_{ab}^2 - \rho F[(B^2 + D_{ab}^2)^{1/2} - \rho B] = 0. \quad (2)$$

TABLE V

Summary of the Fit 1 Analysis

Species	Number of Data	Number of Parameters	σ (kHz)[a]	V_3 (cm^{-1})	Constraint (cm^{-1})	I_α ($uÅ^2$)
CH_3OH–CO	29	15	14.6	182.8	0.020	2.07
CH_3OH–^{13}CO	24	15	14.9	183.5	0.021	2.03
CH_3OD–CO	23	15	7.2	185.2	0.023	2.04
CH_3OD–^{13}CO	19	14	5.1	188.8	0.022	2.15
CD_3OH–CO	21	13	6.7	182.9	-0.013	7.01
CD_3OD–CO	22	13	12.2	182.7	-0.007	7.06

[a] One standard deviation.

This equation can be derived from the definition of the constants involved in terms of the related inertial moments: I_a, I_b, I_{ab}, and I_α, where I_α is the moment of inertia of the top with respect to its symmetry axis, with typical values of 3.2 $uÅ^2$ for CH_3 and 6.4 u $Å^2$ for CD_3. Table V shows the values of this "constraint" determined for the left side of Eq. (2) (in cm^{-1}) and the derived values for I_α for the six isotopic species studied. The values derived for I_α demonstrate an inconsistency in the fits based on their deviation from typical values and cannot be explained by any physical mechanism, e.g., the structural relaxation known as torsional flexing (*37*). This effect normally is modeled with a reduced rotational constant, F, which is dependent on the angle α.

We now have two alternate approaches to examine. The first of these is to use the constraint given by Eq. (2) directly in the fits. This constraint establishes a fixed relationship between five parameters of the Hamiltonian, meaning that they are not independent. In practice, this can be accomplished by calculating D_{ab} from the values of A, B, ρ, and F. Then Eq. (2) may be rewritten as

$$D_{ab}^4 - D_{ab}^2(2AB + 2\rho^2FB + \rho^2F^2) + [(AB + \rho^2FB)^2 - \rho^2F^2B^2] = 0. \quad (3)$$

The four solutions then are

$$D_{ab} = \pm\sqrt{\frac{y \pm \sqrt{y^2 - 4[(AB + \rho^2FB)^2 - \rho^2F^2B^2]}}{2}} \quad (4)$$

where,

$$y = 2AB + 2\rho^2FB + \rho^2F^2.$$

The second route to follow involves fixing I_α to the methanol value. This type of restriction has been used frequently in microwave studies in which a limited set of transitions was obtained. The I_α enters in the definition of ρ and F, as do I_a, I_b, and I_{ab}. The easiest way to treat I_α as a fixed value is to derive the inertial moments from the fitted rotational constants and then use these values plus the fixed value of I_α to calculate F and ρ.

We have implemented both options in the IAM programs. Beginning with the constraint of Eq. (2) and the constants obtained in Fit 1, excluding D_{ab}, which is now

TABLE VI

Summary of the Fit 2 Analysis

Species	Number of Parameters	σ (kHz)[a]	V_3 (cm^{-1})	Constraint (cm^{-1})	I_α ($uÅ^2$)	D_{ab}[b]	I_α[c] ($uÅ^2$)
CH_3OH-CO	14	16.2	175.9	0.020	2.07	-0.0931	3.20
CH_3OH-^{13}CO	14	13.7	176.6	0.021	2.03	-0.0924	3.20
CH_3OD-CO	14	8.6	202.5	0.023	2.04	-0.0924	3.20
CH_3OD-^{13}CO	14	14.7	205.3	0.022	2.15	-0.0884	3.20
CD_3OH-CO	12	6.9	148.9	-0.013	7.01	-0.0850	6.414
CD_3OD-CO	14	12.7	172.8	-0.007	7.06	-0.0839	6.383

[a] One standard deviation obtained in the least-squares fit.
[b] Calculated from Eq. (3) in text.
[c] Calculated from the expression for ρ in terms of the inertial moments.

calculated for each iteration, essentially the same constants employed in Fit 1 were then fit. Due to high correlation between F with V_3, in this case it was necessary to vary F and B by hand due to the fact that the initial constants were too far from the minimum for the fits to converge because of the change in D_{ab}. The results of Fit 2 are summarized in Table VI. Of the four possible values for D_{ab}, the best fits were obtained with the terms in Eq. (4) prefixed with minus signs. The results show two dramatic changes in the set of constants resulting from this analysis when compared to Fit 1. First, there is a large change in the value of D_{ab} for the four isotopic species containing CH_3, while D_{ab} remains close to the Fit 1 value for the species with the CD_3 group as shown in Table V. On the other hand, the barrier, V_3, is now quite different for each of the isotopic species as shown in Table V.

The second approach described above, i.e., fixing I_α at the values for methanol, means that F and ρ are calculated instead of D_{ab}. To achieve this, we fixed D_{ab} at the values determined in Fit 2 since these provided more stable fitting. This analysis (Fit 3) led to the barrier and Eq. (2) constraint values listed in Table VII. The barriers remain quite different between each of the isotopic species and similar to the Fit 2 results, however, the constraint condition fulfilled exactly. Fit 3 is nearly equivalent to Fit 2 with quite small differences in the F and ρ values between them.

TABLE VII

Summary of the Fit 3 Analysis

Species	Number of Parameters	σ (kHz)[a]	V_3 (cm^{-1})
CH_3OH-CO	14	16.8	176.0
CH_3OH-^{13}CO	14	15.0	176.6
CH_3OD-CO	14	8.8	202.5
CH_3OD-^{13}CO	14	8.8	205.3
CD_3OH-CO	12	17.3	148.3
CD_3OD-CO	14	15.2	173.1

[a] One standard deviation obtained in the least-squares fit.

From the analysis discussed above we conclude that several sets of parameters will give a minimum standard deviation. This is primarily due to the limited data set compared to the number of parameters required. In Fit 1, the obtained minimum does not have physical meaning since the I_α values differ too greatly from those of CH_3OH and CD_3OH, and the presence of a weakly bound CO group should not distort the CH_3 group. On the other hand, the constraints imposed in Fits 1 and 2 are probably too stringent. The Eq. (2) restriction is analogous to the moment of inertia condition used for planar molecules in the sense that it should be fulfilled exactly only if there were no vibrational contributions to the moments of inertia. In a similar way, the I_α value could change slightly due to the influence of the CO group and vibrational motions. A change in I_α implies a change in both F and ρ, and consequently a change in the barrier, since what is meaningful for the energy levels is the ratio $s = 4V_3/9F$.

As a final variation of the analysis we iterated fixed values of F and fitted the remaining constants, including ρ and D_{ab}. The best results were obtained starting from the constants of Fit 3, where we used the F value from Fit 1. The resulting barriers for Fit 4 are listed in Table VIII and are close to those obtained in Fit 1. In addition, the I_α values calculated from ρ are very close to those for methanol, and the constraint from Eq. (2) is fulfilled rather well. In this case the F and V_3 parameters are basically independent of the other constants. The problems with Fit 1 are due to poor values of D_{ab}, or stated in another way, the axes defined by the constants of Fit 1 lacked physical sense, since the IAM method is based on an axis system related to the top and the frame. Thus, from an erroneous axis system, wrong I_α values were obtained. The problem with Fit 2 and Fit 3 is the stringent constraints imposed by Eq. (2) and fixed I_α values, respectively.

We conclude that the constants obtained in Fit 4 give the best effective parameters for the IAM Hamiltonian employed here. These effective constants are summarized in Table IX. Although we have not been able to fit the spectra of all the isotopic species to the experimental uncertainty, a consistent set of parameters has been obtained for all species, and for three of these the standard deviation is nearly equal to the experimental error. Table X shows the inertial moments obtained after diagonalizing the inertia matrix and the effective inertial defect, $\Delta = I_c - I_a - I_b$. Except for the anomalous value for CD_3OH–CO, these parameters are consistent with a planar heavy atom equilibrium structure, although some anomalies remain. For example, I_b and I_c

TABLE VIII

Summary of the Fit 4 Analysis

Species	Number of Parameters	σ (kHz)[a]	V_3 (cm^{-1})	Constraint (cm^{-1})	I_{cc} ($uÅ^2$)	D_{ab}[a]
CH_3OH-CO	13	16.1	183.0	-0.0017	3.197	-0.0931
CH_3OH-^{13}CO	13	13.8	183.8	-0.0017	3.200	-0.0924
CH_3OD-CO	12	8.4	185.5	-0.0037	3.203	-0.0924
CH_3OD-^{13}CO	12	6.7	188.8	+0.0027	3.272	-0.0884
CD_3OH-CO	12	6.7	182.8	-0.0129	7.009	-0.0850
CD_3OD-CO	13	12.2	182.7	-0.0074	7.114	-0.0839

[a] One standard deviation obtained in the least-squares fit.

TABLE IX

Rotational Constants for CH_3OH–CO, CH_3OH–^{13}CO, CH_3OD–CO, and CH_3OD–^{13}CO

Parameter	CH_3OH–CO	CH_3OH–^{13}CO	CH_3OD–CO	CH_3OD–^{13}CO	CD_3OH–CO	CD_3OD–CO
A	28217.32(13)[a]	28220.29(10)[a]	27702.41(6)[a]	27795.29(9)[a]	22225.33(27)[a]	21833.3(5)[a]
B	2142.44(36)	2121.66(36)	2144.60(20)	2098.4(14)	2149.92(63)	2172.0(11)
C	1757.14(29)	1742.14(26)	1757.80(17)	1742.1(147)	1659.28(60)	1653.5(9)
Δ_{ab}	-2789.84[b]	-2771.61[b]	-2771.24[b]	-2651.81[b]	-	-
Δ_J	0.01685(63)	0.01652(54)	0.01902(6)	0.01912(16)	0.02804(6)	0.02684(5)
Δ_{JK}	-10.999(93)	-10.556(93)	-6.811(72)	-7.57(16)	-0.856(91)	-0.75(18)
δ_J	-0.00326(54)	-0.00327(42)	-	-	-0.00498(6)	-0.00527(6)
F_v	60.6(45)	57.65(39)	50.25(20)	54.94(31)	12.1(12)	-4.0(27)
α_v	6.56(13)	6.57(12)	5.77(12)	6.30(28)	2.6(6)	1.6(12)
c_2	36.1(11)	35.3(11)	41.14(68)	45.9(56)	60.1(27)	38.9(44)
c_4	15.2(11)	15.47(81)	8.28(13)	7.50(36)	-	-
k_5	-36.15(33)	-34.54(33)	-22.28(26)	-25.12(62)	-	-
ρ	0.094705(24)	0.094670(26)	0.093553(19)	0.0990(14)	0.1511[b]	0.1497[b]
V_3 (cm^{-1})	183.049(15)	183.779(16)	185.491(12)	189.32(92)	183.22(15)	182.79(21)
F (cm^{-1})	5.7590[b]	5.7590[b]	5.2254[b]	5.2254[b]	3.4267[b]	3.0459[b]

[a] Uncertainty refers to the last digits shown and are one standard deviation. The values shown are in MHz unless specifically noted.

[b] These constants were fixed at the value given (see text for details).

for CH_3OD–CO are smaller than those for CH_3OH–CO, and a similar situation occurs for the CD_3OH and CD_3OD species. Due to the large number of parameters required to fit the relatively small data set, the molecular parameter should be considered as "effective" molecular constants within the model framework chosen.

V. STRUCTURE

Due to the anomalies in the moment of inertia data derived in the internal rotation analysis, we elected to use the rotational analysis of the *A* state as the basis for structure determination. The structure we report here is based on fitting the moments of inertia, I_a and I_b, of each observed isotopic species in a least-squares manner to a geometry based on the assumption that the monomer geometries do not change in the complex.

TABLE X

Moments of Inertia and Inertial Defect from the Fit 4 Analysis (in u $Å^2$)

Species	I_a	I_b	I_c	I_α	Δ $(I_c-I_a-I_b)$
CH_3OH–CO	17.725	273.600	287.616	3.197	-3.708
CH_3OH–^{13}CO	17.726	276.080	290.094	3.200	-3.711
CH_3OD–CO	18.050	273.537	287.904	3.203	-4.077
CH_3OD–^{13}CO	18.007	276.410	290.234	3.272	-4.182
CD_3OH–CO	22.326	290.719	304.588	7.010	-8.457
CD_3OD–CO	22.702	289.805	305.701	7.114	-6.807

The small negative inertial defect for CH_3OH–CO (-0.726 u Å^2) suggests that the heavy atoms are most likely coplanar, but it also shows a substantial positive contribution due to the deviation from the typical value of -3.2 u Å^2 for a methyl group alone. The change in inertial defect of -0.074 u Å^2 between the normal isotopic form and CH_3OH–^{13}CO indicates that the C atom of CO is coplanar with the heavy atom frame of methanol. A comparison of the inertial defects shown in Table IV for the two CH_3OD–CO and $-^{13}CO$ species lends further support to this conclusion. While the change in inertial defect between analogous species containing the OH group versus the OD group on the order of -0.1 u Å^2 might be interpreted as a nonplanar OH hydrogen, it might also result from a change in zero point large-amplitude bending vibrations. By employing the usual assumption that the monomer geometries are unchanged in complex formation, only three structural parameters are required if the heavy atoms lie in a plane. These are R_{cm} and the two angles θ and ϕ as defined in Fig. 2; here R_{cm} is defined as the distance between the center of mass of CO and a point on the methanol C–O bond 0.7302 Å from the C atom, which is the a coordinate of the center of mass of methanol. Fits were carried out using the I_a and I_b and I_a and I_c moments of inertia, resulting in one standard deviation values of 0.17 and 0.21 u Å^2, respectively. The derived parameters for the two fits are $R_{cm} = 4.153(1)$ Å, $\theta = 108.8(9)°$, and $\phi = 4.5° \pm 8.2°$ for the I_a, I_b fit and $R_{cm} = 4.171(1)$ Å, $\theta = 109.9(8)°$, and $\phi = 6° \pm 13°$ for the I_a, I_c combination, which is essentially the geometry depicted in Fig. 2. The slightly better fit with the I_a, I_b moments provides a distance of 2.44(4) Å between the hydroxyl hydrogen atom and the carbon atom of CO and a distance of 3.16(4) Å from the carbon atom of CO to the nearest methyl hydrogen atom, which was assumed to lie in the heavy atom plane. Clearly CH_3OH–CO does not provide a linear hydrogen bond or even a clear directional character, particularly when compared to the water–carbon monoxide complex (*30*).

VI. DISCUSSION

We report here the microwave spectrum of six isotopic forms of the methanol–carbon monoxide complex, which exhibits rather large internal rotation splitting from methyl torsion. The moments of inertia derived from the rotational constants were employed in the structural analysis, and a geometry of modest accuracy has been determined. In order to fit the observed rotational spectra to near-measurement ac-

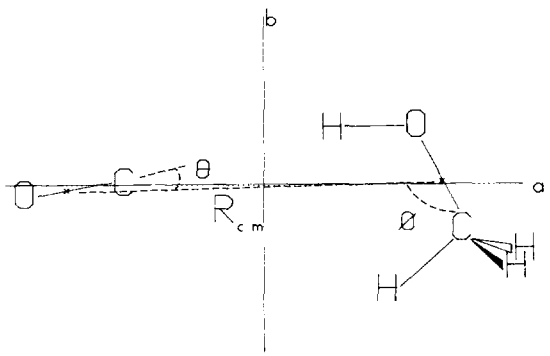

FIG. 2. Definition of the structural parameters for the methanol–carbon monoxide complex.

curacy an extended IAM treatment was necessary, but due to either limitations in the spectral data or some model error this analysis must be considered to provide "effective" molecular parameters such as the V_3 potential barrier.

Our literature search revealed only one recent ab initio structure study of CH_3OH–CO by Latajka *et al.* (*38*). These workers found the lowest energy form to have a linear hydrogen bond between the hydroxyl H of methanol and the carbon atom of CO with the approximate conformation determined here from experiment. While specific geometric parameters were not given, the authors indicate the distance from the oxygen atom of methanol to the nearest atom of CO was about 3.5 Å for each of the conformations examined. This distance agrees moderately well with the experimental value of 3.36 Å, while the largest discrepancy occurs in the angular orientation of the two units. The CO–H_2O complex is the closest analogous species with an experimentally determined structure. In this case a linear hydrogen bond (H–C) has been found with the O–C distance of 3.347 Å (for D_2O–CO), and a hydrogen bond distance of 2.41 Å is derived, compared to 3.36 and 2.44 Å, respectively, for methanol–carbon monoxide. As a means of estimating the relative strength of weak hydrogen (or van der Waals) bonds, the pseudo-diatomic model (*39*) is often invoked when calculating the stretching force constant, k_s. For CH_3OH–CO we determined that $k_s = 1.4$ N m^{-1}, which may be compared to a value of 2.74 Nm^{-1} for H_2O–CO (*30*). A number of OC–H*X* complexes have been studied which show a stronger hydrogen bond than either water–CO or methanol–CO, namely OC–HCN (3.3 Nm^{-1}) (*40*), OC–HBr (3.0 Nm^{-1}) (*41*), and OC–HCl (4.5 Nm^{-1}) (*42*). Thus, it is apparent that methanol has the weakest bond among these CO complexes and has a stretching force constant comparable with the linear bonded HCCH–CO, 1.7 Nm^{-1} (*43*). Rather interestingly, the methyl-substituted form of acetylene–CO, i.e., CH_3CCH–CO, is not linear H-bonded but has a slipped parallel structure (*44*), and methanol–CO appears to have a conformation between these two geometries.

The value of $V_3 = 183$ cm^{-1} reported here is about a factor of two smaller than that for methanol (373 cm^{-1}), which is a surprisingly large change to attribute to changes in electron density in the methanol subunit considering the weakness of the bonding interaction. Only one other methanol complex has been studied wherein the internal rotation has also been treated, methanol–formamide (*45*), with a value $V_3 = 231.0$ cm^{-1}. The barrier for formamide–methanol is 50 cm^{-1} higher than the barrier for methanol–CO, while the short bonding distance between OH and formamide, about 2 Å, suggests a much stronger interaction between methanol and formamide, which adds to the perplexity of interpreting these effective barriers. Some of the present authors have suggested that a large-amplitude motion of the OH group within the complex could provide an additional term in describing the internal rotation of the methyl group which might explain this apparent barrier reduction (*46*). There remains insufficient spectral information to examine this idea further since information on torsionally excited states of the complex would be most sensitive to this motion.

Several additional complexes containing methanol are currently under study in our laboratory, namely $(CH_3OH)_2$ and CH_3OH–HCN, and both of these species have effective V_3 barriers in the 100 to 200 cm^{-1} region (*47*). Thus, large internal rotation effects seem to be fairly common in dimeric complexes of methanol. Understanding the origin of these effects has important implications in condensed-phase chemistry and biological systems since reaction rates may be substantially modified by cooperative effects of the hydrogen bonding in systems containing methyl rotors.

As described in the Introduction, the objective of this study is to determine the structural conformation of methanol–CO and several other methanol complexes which are considered as important intermediates in the MTG process. Once the structures of the dimeric species are well established, studies of these dimeric complexes with a strong acid such as HF will be undertaken to determine if the CH_3OH–X dimer structure is substantially modified when HF is incorporated in the trimeric complex.

ACKNOWLEDGMENT

J.O. is grateful to the Spanish Consejo Superior de Investigaciones Científicas for a postdoctoral grant.

RECEIVED: April 26, 1994

REFERENCES

1. C. D. CHANG, *Catal. Rev.* **25,** 1–118 (1983).
2. S. L. MEISEL, J. P. MCCULLOUGH, C. H. LEUHTHALER, AND P. B. WEIS, *Chemtech* **6,** 86–89 (1984).
3. C. D. CHANG, "Hydrocarbons from Methanol," Dekker, New York, 1983.
4. D. E. PEARSON, *J. Chem. Soc. Chem. Commun.,* 397 (1974).
5. P. SALVADOR AND W. KLADNIG, *J. Chem. Soc. Faraday Trans. 1* **73,** 1153–1168 (1977).
6. Y. ONO AND T. MORI, *J. Chem. Soc. Faraday Trans. 1* **77,** 2209–2221 (1981).
7. G. A. OLAH, *Pure Appl. Chem.* **53,** 201–207 (1981).
8. G. A. OLAH, H. DOGGWEILER, J. D. FLEBERG, S. FROLICH, M. J. GRDINA, R. KARPELS, T. TEUMI, S. INABA, W. M. IP, K. LAMMERTSA, G. SALEM, AND D. C. TABOR, *J. Am. Chem. Soc.* **106,** 2143–2149 (1984).
9. G. A. OLAH AND R. H. SCHLOSBERG, *J. Am. Chem. Soc.* **90,** 2726–2727 (1968).
10. G. A. OLAH, G. KLOPMAN, AND R. H. SCHLOSBERG, *J. Am. Chem. Soc.* **91,** 3261–3268 (1969).
11. P. RIMMELIN, H. TAGHAVI, AND J. SOMMER, *J. Chem. Soc. Chem. Commun.,* 1210–1211 (1984).
12. D. KAGI, *J. Catal.* **69,** 242–243 (1981).
13. T. BABA, J. SAKAI, H. WATANABE, AND Y. ONO, *Bull. Chem. Soc. Jpn.* **55,** 2555–2559 (1982).
14. C. D. CHANG AND A. J. SILVESTRI, *J. Catal.* **47,** 249–259 (1977).
15. C. D. CHANG AND C. T.-W. CHU, *J. Catal.* **74,** 203–206 (1982).
16. P. B. VENUTO AND P. S. LANDIS, *Adv. Catal.* **18,** 259–371 (1968).
17. F. A. SWABB AND B. C. GATES, *Ind. Eng. Chem. Fundam.* **11,** 540–545 (1972).
18. J. E. JACKSON AND F. M. BERTSCH, *J. Am. Chem. Soc.* **112,** 9085–9092 (1990).
19. E. J. MUNSON, N. D. LAZO, M. E. MOELLENHOFF, AND J. F. HAW, *J. Am. Chem. Soc.* **113,** 2783–2784 (1991).
20. J. Z. GILLIES, C. W. GILLIES, R. D. SUENRAM, AND F. J. LOVAS, *J. Am. Chem. Soc.* **110,** 7991–7999 (1988).
21. J. Z. GILLIES, C. W. GILLIES, R. D. SUENRAM, F. J. LOVAS, AND W. STAHL, *J. Am. Chem. Soc.* **111,** 3073–3074 (1989).
22. J. Z. GILLIES, C. W. GILLIES, F. J. LOVAS, K. MATSUMURA, R. D. SUENRAM, E. KRAKA, AND D. CREMER, *J. Am. Chem. Soc.* **113,** 6408–6415 (1991).
23. J. Z. GILLIES, C. W. GILLIES, F. J. LOVAS, AND R. D. SUENRAM, *J. Am. Chem. Soc.* **115,** 9253–9262 (1993).
24. N. W. HOWARD AND A. C. LEGON, *J. Chem. Phys.* **88,** 4694–4701 (1988).
25. G. T. FRASER, K. R. LEOPOLD, D. D. NELSON, JR., A. TUNG, AND W. KLEMPERER, *J. Chem. Phys.* **80,** 3073–3077 (1984).
26. M. A. DVORAK, R. S. FORD, R. D. SUENRAM, F. J. LOVAS, AND K. R. LEOPOLD, *J. Am. Chem. Soc.* **114,** 108–115 (1992).
27. F. J. LOVAS AND R. D. SUENRAM, *J. Chem. Phys.* **87,** 2010–2020 (1987).
28. R. D. SUENRAM, F. J. LOVAS, G. T. FRASER, J. Z. GILLIES, C. W. GILLIES, AND M. ONDA, *J. Mol. Spectrosc.* **137,** 127–137 (1989).
29. T. J. BALLE AND W. H. FLYGARE, *Rev. Sci. Instrum.* **52,** 33–45 (1981).
30. D. YARON, K. I. PETERSON, D. ZOLANDZ, W. KLEMPERER, F. J. LOVAS, AND R. D. SUENRAM, *J. Chem. Phys.* **92,** 7095–7109 (1990).

31. F. J. LOVAS, R. D. SUENRAM, M. TRETYAKOV, S. BELOV, AND W. STAHL, in preparation.
32. J. K. G. WATSON, *in* "Vibrational Spectra and Structure" (J. R. Durig, Ed.), Vol. 6, pp. 1–88, Elsevier, Amsterdam, 1977.
33. I. KLEINER, M. GODEFROID, M. HERMAN, AND A. R. W. MCKELLAR, *J. Mol. Spectrosc.* **142,** 238–253 (1990).
34. I. KLEINER, J. T. HOUGEN, R. D. SUENRAM, F. J. LOVAS, AND M. GODEFROID, *J. Mol. Spectrosc.* **148,** 38–49 (1991).
35. I. KLEINER, J. T. HOUGEN, R. D. SUENRAM, F. J. LOVAS, AND M. GODEFROID, *J. Mol. Spectrosc.* **153,** 578–586 (1992).
36. W. LIANG, J. G. BAKER, E. HERBST, R. A. BOOKER, AND F. C. DELUCIA, *J. Mol. Spectrosc.* **120,** 298–310 (1986).
37. R. M. LEES, *J. Chem. Phys.* **59,** 2690–2697 (1973).
38. Z. LATAJKA, H. RATAJCZAK, J. MURTO, AND W. J. ORVILLE-THOMAS, *J. Mol. Struct.* **194,** 45–60 (1989).
39. D. J. MILLEN, *Can. J. Chem.* **63,** 1477–1479 (1985).
40. E. J. GOODWIN AND A. C. LEGON, *Chem. Phys.* **87,** 81–92 (1984).
41. M. R. KEENAN, T. K. MINTON, A. C. LEGON, T. J. BALLE, AND W. H. FLYGARE, *Proc. Natl. Acad. Sci. USA* **77,** 5583–5587 (1980).
42. P. D. SOPER, A. C. LEGON, AND W. H. FLYGARE, *J. Chem. Phys.* **74,** 2138–2142 (1981).
43. A. C. LEGON, A. L. WALLWORK, J. W. BEVAN, AND Z. WANG, *Chem. Phys. Lett.* **180,** 57–62 (1991).
44. F. J. LOVAS, P. W. FOWLER, Z. KISIEL, S-H. TSENG, R. D. BECK, D. F. EGGERS, T. A. BLAKE, AND R. O. WATTS, submitted for publication.
45. F. J. LOVAS, R. D. SUENRAM, G. T. FRASER, C. W. GILLIES, AND J. ZOZOM, *J. Chem. Phys.* **88,** 722–729 (1988).
46. G. T. FRASER, F. J. LOVAS, AND R. D. SUENRAM, *J. Mol. Spectrosc.* **167,** 231–235 (1994).
47. F. J. LOVAS, private communication.